Journal of Materials Chemistry A

ROYAL SOCIETY OF CHEMISTRY

PAPER

View Article Online
View Journal | View Issue

Cite this: J. Mater. Chem. A, 2023, 11, 6403

Simultaneous tailoring of hydrogen evolution and dendrite growth *via* a fertilizer-derived additive for the stabilization of the zinc anode interface†

Mahammad Rafi Shaik,[a] Syryll Maynard Olidan,[a] Jihoon Kim, *[a] Kuk Young Cho *[b] and Sukeun Yoon *[a]

Zinc metal anodes suffer from unavoidable issues related to their charge–discharge stability (mainly inducing uneven dendrite formation and unwanted side reactions between the electrode and electrolyte), which lead to their inferior reversibility and hinder their commercial applications. Optimizing the nucleation behavior to improve reversible Zn electrodeposition has been extensively studied, but the poor cycling reversibility and additive cost remain challenging. Herein, an additive engineering approach using fertilizer-derived *N*-methylthiourea was designed to regulate the Zn-electrolyte interface while avoiding these problems. This sulfur-carrying urea molecule has a strong affinity for both Zn and Zn^{2+}, and it preferentially adsorbs on the Zn surface to delay water adsorption and controls the secondary diffusion of Zn^{2+} to stabilize the Zn/electrolyte interface, extending the hydrogen evolution potential to −0.92 V. It also prolongs the induction time of Zn crystal formation, leading to uniform Zn plating/stripping as well as dendrite formation suppression. Consequently, the electrochemical performance was greatly improved in the Zn|Zn symmetric cell, showing a low overvoltage (40 mV) and stable cycling performance (1000 h) at 1 mA cm^{-2}. Further, the Zn|V_2O_5–C full-cell delivered a consistent capacity over 420 cycles with a coulombic efficiency of ∼98.6%. This study demonstrates a new strategy for metal–electrolyte interface stabilization that can be applied to practical metal-based batteries.

Received 21st December 2022
Accepted 20th February 2023

DOI: 10.1039/d2ta09913f

rsc.li/materials-a

1 Introduction

Li-ion batteries (LIBs), corresponding to various rechargeable battery technologies, have achieved great commercial success in portable electronics, electric vehicles (EVs), and grid-scale energy-storage systems (ESSs) due to their excellent electrochemical performance.[1,2] However, technical challenges in terms of their intrinsic safety and reliability, together with concerns about limited lithium resources are driving the development of new batteries.[3] From this point of view, lithium-free Zn-ion batteries are attracting tremendous attention as next-generation energy-storage devices because of their non-inflammability, environmental compatibility, high theoretical capacity (820 mA h g^{-1} or 5850 mA h cm^{-3}), earth-abundant material, low redox potential (−0.76 V *vs.* SHE), and Li-ion battery manufacturing facility usability.[4–6] Nevertheless, Zn-ion batteries have the distinct disadvantage of a poor charge–discharge reversibility because of the corrosion reaction and Zn dendrite formation caused by the hydrogen evolution reaction (HER), electrochemically inactive by-products (ex. ZnO, $Zn(OH)_2$, and $ZnSO_4[Zn(OH)_2]_3 \cdot xH_2O$), and non-uniform Zn electrodeposition.[7]

Various strategies have been proposed in recent years to improve the reversible performance of Zn-ion batteries, including the use of artificial functional layers, separator designs, and liquid- and/or solid-electrolyte engineering.[8–12] First, artificial layers composed of a polymer or inorganic composite restrict the contact between the electrolyte and the Zn electrode and even induce Zn-ion transport, thereby improving the coulombic efficiency and cycling performance.[13–16] Second, a powerful multifunctional separator can modulate the Zn-ion-transport behavior and simultaneously improve the Zn metal anode performance as a physical barrier to the growth of Zn dendrites.[17–19] Finally, a simple way to adjust the chemical composition of the electrolyte can have a direct and intrinsic effect on Zn-ion transport, interfacial chemistry, dendrite-free Zn deposition, and cell performance.[20–22] The use of aqueous solution electrolytes for Zn-ion batteries is advantageous in terms of safety and affordability. However, it is also disadvantageous; alkaline electrolytes with low hydrogen evolution potentials can produce zinc hydroxide *via* hydrolysis and eventually passivate the Zn metal

[a]Division of Advanced Materials Engineering & Institute for Rare Metals, Kongju National University, Chungnam 31080, Republic of Korea. E-mail: jihoon.kim@kongju.ac.kr; skyoon@kongju.ac.kr

[b]Department of Materials Science and Chemical Engineering, Hanyang University, Gyeonggi 15588, Republic of Korea. E-mail: kycho@hanyang.ac.kr

† Electronic supplementary information (ESI) available. See DOI: https://doi.org/10.1039/d2ta09913f

surface with inactive zinc oxide. Therefore, the Zn-ion batteries currently under study use mildly acidic or neutral electrolytes to alleviate the formation of passivation by-products. However, this produces hydrogen gas during cycling and changes the pH value of the electrolyte to alkaline, which promotes the formation of by-products on the Zn metal surface.[23]

Two alternatives (electrolyte additives and water-starved electrolytes) have been proposed to alleviate the degradation of battery performance using mildly acidic electrolytes, such as the low coulombic efficiency due to hydrogen gas evolution and by-product formation. These can shield the electric field with heterogeneous Zn deposits and control the Zn-ion distribution at the interface by electrostatic interactions. This can reduce the free-water content and suppress side reactions, change the solvated Zn structure, and promote to the growth direction of the Zn crystal.[24–27] Organic additives have a significant effect on the Zn metal surface stabilization. For example, the diethyl ether polarity means it preferentially adsorbs on small-sized Zn protrusions, thereby locally shielding the electric field and blocking the electrodeposition of additional Zn ions.[28] Some positively charged amino acids and tetrabutylammonium sulfate (TBA_2SO_4) were adsorbed on the Zn metal surface to form a self-adapting Zn-electrolyte interface, which inhibited water adsorption and led to uniform Zn deposition.[29,30] In addition, sodium dodecyl sulfate (SDS), polyethylene glycol (PEG-8000), cetyltrimethylammonium bromide (CTAB), and dimethyl sulfoxide (DMSO) stabilizers for Zn plating could improve the Zn metal surface by changing the crystal direction of Zn electrodeposition and decreasing the corrosion.[31–33] Except for electrolyte additives, the method used for controlling the water content in the electrolyte can suppress side reactions induced by water as well as the desolvation energy caused by the interaction between water and Zn ions. A large number of anions in the electrolyte with high concentrations of $Zn(TFSI)_2$, $Zn(ClO_4)_2$, or $ZnCl_2$ can migrate around the Zn ions to form compact ion pairs, which can significantly alter the configuration of the typical $[Zn–(H_2O)_6]^{2+}$, reducing the hydration of Zn ions and the formation of a passivation layer.[34–36] In addition, using a gel-type semi-solid electrolyte containing gelatin rather than a liquid electrolyte is an effective method for improving the electrochemical performance that works by weakening the influence of water on the Zn metal anode.[37,38]

This study investigated the interfacial modulation effect of fertilizer-derived *N*-methylthiourea (MTU) adsorption in a mildly acidic electrolyte on the electrochemical properties of Zn-ion batteries with the aim of suppressing dendritic Zn and obtaining smooth deposits. As one of the various inorganic and organic additives, including organic gelatin, polyethylene glycol, thiourea, and ionic liquids, for Zn electrodeposition, the easily available and inexpensive MTU acts in a manner similar to leveling and brightening agents in Zn electroplating baths to improve the physicochemical properties of Zn deposits.[39,40] It reduces the grain size, changes the default growth direction of Zn crystals, and inhibits the formation of Zn nucleation on the electrode surface by readily adsorbing to rapidly grow the number of active sites through the coordination of sulfur atoms. This implies that MTU could potentially be used as a functional additive to change the Zn electrodeposition behavior. We believe that this study provides valuable information for the further advancement of electrolyte additive technology for the commercial application of metal-based battery systems through restricting dendrite growth and improving the solid-electrolyte interface (SEI) by regulating the nucleation and crystal growth.

2 Experimental

2.1 Electrolyte preparation

An aqueous solution containing 1 M $ZnSO_4$ was used as the base electrolyte. All the chemical reagents were analytically pure and purchased from Alfa Aesar. The desired amount of *N*-methylthiourea (MTU) (Fig. S1†) was dissolved in base electrolyte as an additive.

2.2 Synthesis of the V_2O_5–C composite cathode

The V_2O_5–C composite cathode material used in a full cell was prepared by mechanical ball milling. A mass ratio of 8 : 2 V_2O_5 and carbon black was ball-milled for 180 min at 300 rpm using 316 L stainless steel balls (diameters: 10 and 5 mm) in 80 cm^3 steel vials under an Ar atmosphere.

2.3 Material characterization

The crystalline phases of Zn deposits were investigated by X-ray diffraction (XRD; Rigaku SmartLab, Cu Kα radiation). The morphology, microstructure, and composition were determined by field-emission scanning electron microscopy (FE-SEM; Carl Zeiss, SIGMA 500) combined with energy-dispersive X-ray spectroscopy (EDS; Bruker, XFlash 6130). The chemical composition of the surface was characterized by X-ray photoelectron spectroscopy (XPS; Thermo Fisher Scientific, K-α, Al Kα radiation). The interaction between the Zn ions and MTU was characterized by Fourier transform infrared (FTIR) spectroscopy (PerkinElmer Spectrum 100). The cells were disassembled using a coin cell disassembly tool (Hohsen Corp.) after cycling to investigate the Zn metal surfaces. The contact angle was analyzed using an SEO Phoenix 300 system from an average of five measurements performed by dropping 14 μL of the electrolyte at different locations. Real-time experiments of Zn plating/stripping were performed using a lab-made *in situ* symmetric cell, and snapshots were recorded using a digital camera-induced optical microscope (Siwon Optical, Dimis-M5). The pH of the electrolytes was measured using an Ohaus Starter 2100 pH meter. The zeta potentials were measured using a Malvern Zetasizer Nano ZSP. The viscosities were recorded using an AND SV-A series viscometer. The ionic conductivities of the electrolytes were established using a data recorder consisting of two platinum electrodes (WTW Cond 3110).

2.4 Electrochemical measurements

Chronopotentiometry measurements were used to evaluate the Zn plating/stripping properties in Zn symmetric cells at a constant current density of 1 mA cm^{-2} using a battery cycler (Maccor 4000). The cathode was prepared by mixing 80 wt%

V_2O_5–C composite, 10 wt% carbon black (Super P), and 10 wt% PVDF-HFP in NMP to form a slurry. This slurry was coated on 304 stainless steel foil (12 μm thickness) and dried at 60 °C for 3 h under vacuum to provide an electrode with a loading of ~4 mg cm^{-2}. A coin cell (CR2032) was assembled using a Zn metal anode, Whatman glass microfibers as a separator, and an aqueous electrolyte. The galvanostatic charge–discharge tests were performed at 100 mA g^{-1} (with respect to V_2O_5–C) within the voltage window of 1.5–0.8 V *vs.* Zn^+/Zn. The cyclic voltammetry (CV) testing was performed using a LANHE G340A battery tester at various scan rates. Electrochemical impedance spectroscopy (EIS) was conducted using a PARSTAT 4000 apparatus by applying a 10 mV amplitude signal in the frequency range of 10 kHz to 1 Hz. The impedance response was recorded after the 50th cycle and fitted using ZSimpWin software. The Zn ionic transference number (t_{Zn}^{2+}) was calculated from chronoamperometry and EIS results using the Bruce–Vincent–Evans equation. Potentiodynamic polarization and cyclic voltammetry tests were performed on the ZIVE SP2 instrument using a three-electrode system with Zn plate samples (or glassy carbon), graphite (or platinum wire), and a saturated calomel electrode (SCE) as the working, counter, and reference electrodes, respectively. Linear sweep voltammetry was performed on the cells using a PARSTAT 4000 potentiostat/galvanostat. The working electrode was made of stainless steel, with the counter and reference electrodes made of Zn. The scan rate was 1 mV s^{-1}.

3 Results and discussion

The essence of this electrolyte additive strategy is to use the electrostatic absorption of MTU to promote the formation of a uniform interfacial layer on the Zn metal anode. The electrolyte was prepared using 1 M $ZnSO_4$ as the base electrolyte, followed by the addition of a series of MTUs (0.05, 0.1, and 0.5 M). These were no longer dissolved and became almost saturated when the concentration of MTU reached 0.5 M in 1 M $ZnSO_4$-based electrolyte. All the electrolytes with MTU were transparent liquids with flowability (Fig. S2†). In addition, the increase in the oxygen evolution reaction potential determined by linear sweep voltammetry (LSV) at a scan rate of 1 mV s^{-1} in 1 M Na_2SO_4 electrolyte with MTU predicted the protective effect of the MTU additive (Fig. 1a). The zeta potential of the Zn particles increased from −14.9 to 20.2 mV with the addition of MTU (Fig. 1b). This clearly confirmed the electrostatic absorption of MTU molecules on the Zn surface. The cyclic voltammetry (CV) curves of the Zn symmetric cells further illustrated the self-adaptability of the MTU adsorption (Fig. S3†). No specific oxidation/reduction peaks were observed; this indicated that a general capacitive absorption behavior occurred. It could be expected that the self-adapting absorption properties of MTU could influence the Zn plating/stripping reaction by controlling the Zn anode interfacial charge. It was reported that sulfur atoms in thiourea-derivative molecules can act as active centers when adsorbed on the electrode surface, wherein the adsorption intensity is related to the electron-donation ability of the C=S bond and the resistance size of the substituent

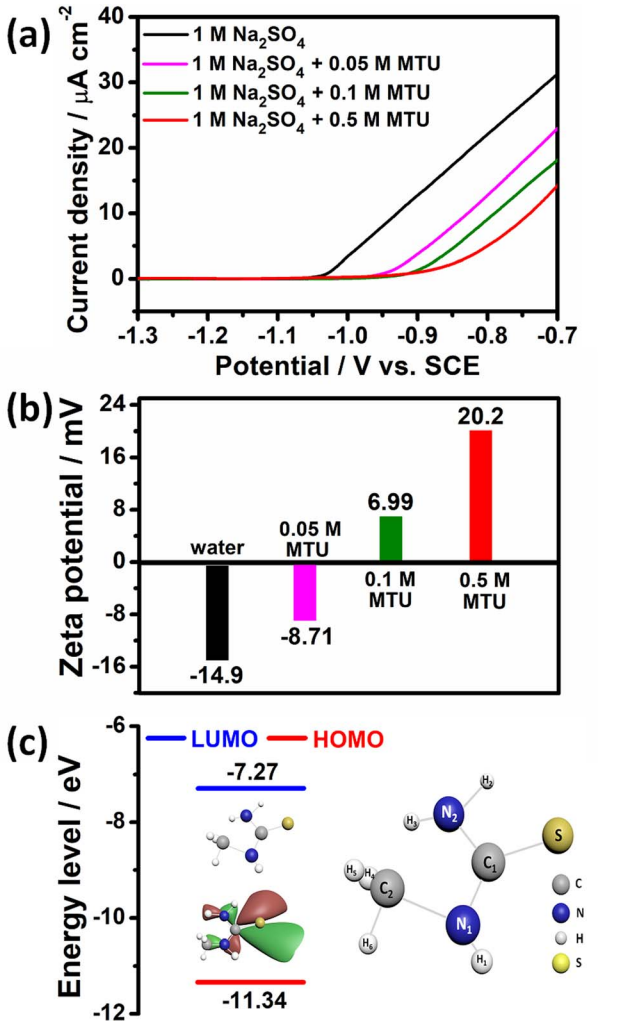

Fig. 1 (a) Linear sweep voltammetry using Zn-metal, graphite, and SCE electrodes. (b) Zeta potential of Zn particles in DI water using various MTU concentrations. (c) HOMO/LUMO diagram and molecular structure of MTU.

group.[41] According to molecular orbital theory, molecular activity is mainly affected by the highest occupied molecular orbital (HOMO) and its surrounding molecular orbitals (Fig. 1c). MTU is an easy additive for allocating electrons to the vacant orbital of Zn metal because the methyl group (–CH_3) is an electron-donating group, which can increase the electronegativity of the sulfur atoms. In addition, replacement of the H-atom of the methyl group in thiourea can extend the C–S bond and promote the adsorption of the additive molecules to the Zn metal surface through the C–S centers. Therefore, the MTU, related to the thiourea substituted with a methyl group, binds to the Zn deposit surface, which can contribute to suppressing the formation of Zn dendrites by steric hindrance of the methyl group as well as the electronic properties.

Linear sweep voltammetry analysis was performed at a scan rate of 1 mV s^{-1} in a three-electrode system using 1 M Na_2SO_4 electrolyte with and without MTU to confirm the reactivity of MTU in interfacial adsorption (Fig. 2a). The onset potential of

the lowest MTU concentration (approximately −1.8 V *vs.* SCE) was much larger than that of the electrolyte without MTU.

Therefore, polarization by the hydrogen evolution reaction (HER) increased, and water adsorption was relatively inhibited. This result was confirmed by simple pH measurements; whereby higher pH values facilitated potential hydrogen evolution in Zn aqueous solution and increased the by-product generation during the discharge process.[42] However, MTU tended to have a lower pH value with increasing its content (Fig. S4†). Meanwhile, the potentiodynamic polarization measured at a rate of 5 mV s^{-1} demonstrated that the corrosion voltage of the MTU electrolyte increased from −0.95 V to over −0.89 V *vs.* Zn^{2+}/Zn compared with the $ZnSO_4$ electrolyte, and the corrosion current density (i_{corr}) decreased from 0.976 to 0.974 mA cm^{-2} (Fig. 2b). This indicated that the tendency for corrosion reactions was low and the side reactions were mitigated. Finally, the impact of MTU adsorption on Zn nucleation and growth was investigated through chronoamperometric tests at a constant potential of −1.43 V (Fig. 2c). Initially, a sharp increase in the current was observed associated with the formation and accumulation of Zn nuclei. Thereafter, the current began to decrease owing to the depletion of active species and/or superposition of growing Zn crystals. Moreover, the maximum current (i_m) values were always greater than those of the electrolyte with MTU, and the i_m values decreased with increasing the MTU concentration. This indicated that the adsorption of MTU molecules could reduce the number of active sites on the exposed electrode surface and prolong the induction time for Zn crystal formation.[43] The chemical stability and nucleation behavior of Zn in the electrolyte containing MTU were further investigated through direct surface observation after Zn metal immersion for 5 days (Fig. 2d). Zn metal in the electrolyte with 0.5 M MTU showed a relatively smooth morphology compared with the $ZnSO_4$ electrolyte. This limited surface corrosion, and also displayed small, densely distributed Zn nucleation growth after several cycles. Among other physical properties, the surface tension of a material is closely related to the affinity between the material and electrolyte, which can directly affect the interfacial resistance and ionic conductivity. The ionic conductivity of the electrolytes slowly decreased from 49.3 to 44.9 mS cm^{-1} as the MTU concentration in the electrolyte was increased between 0.05 and 0.5 M (Fig. S5†). The viscosity of an electrolyte generally increases in proportion to the concentration of the dissolved salt (Fig. S6†). In addition, the ionic conductivity decreased in the electrolyte with a high concentration of dissolved salt, because the movement of ions is slow in a high-viscosity solvent.[44] This is consistent with previous results. That is, increasing the MTU concentration in the electrolyte may increase the number of MTUs adsorbed on the Zn metal surface for nucleation and dendrite control, as shown in Fig. 2a–d; Conversely, there are relative advantages and disadvantages of hindering the movement of Zn ions in the electrolyte and limiting its kinetics, as shown in Fig. S5 and S6.† However, as shown in these figures, an increase in the MTU concentration from 0.05 to 0.5 M had only a small effect on the increase in ionic conductivity. Therefore, a properly adjusted MTU concentration in the electrolyte can maximize the Zn-ion battery performance by optimizing the amount of MTU adsorption on the Zn metal surface while reducing the effect of the decreasing ionic conductivity. Fig. S7† presents the chronoamperometry curve of the dummy cell (Zn symmetric cell) at a polarization voltage of 10 mV, while Fig. S8† shows the Nyquist plots before and after polarization. The Zn ionic transference numbers ($t_{Zn^{2+}}$) were 0.47 and 0.48 with and without 0.5 M MTU electrolytes, respectively. The slightly lower value for the MTU-containing electrolytes was probably due to the Zn-ion-transport interference by the MTU, and this decrease was responsible for the slightly lower ionic conductivity of the

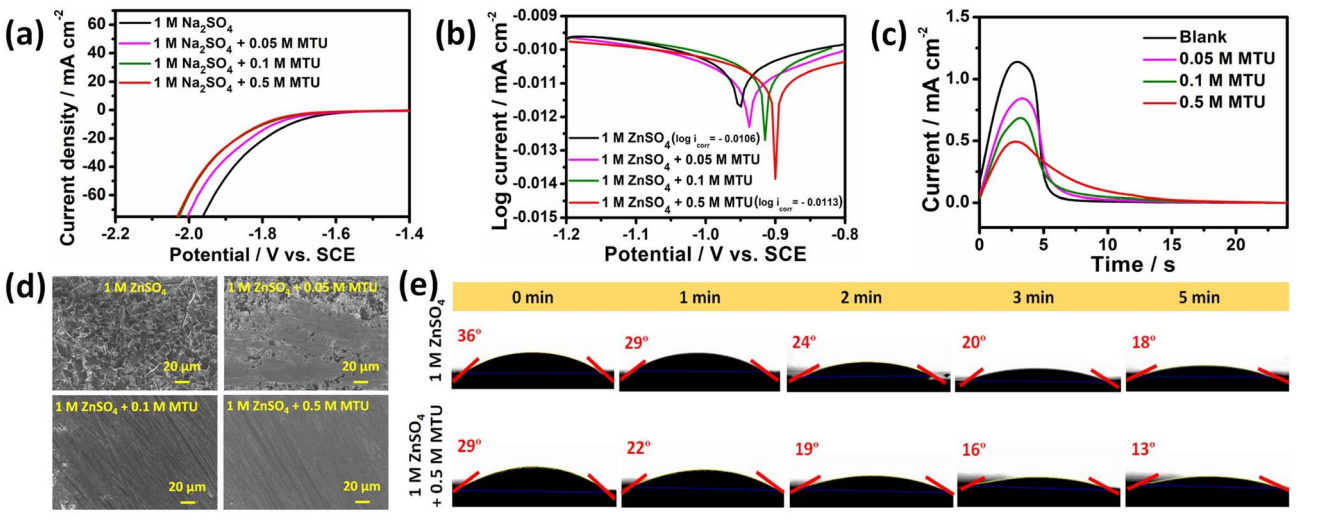

Fig. 2 (a) Linear sweep voltammetry, (b) potentiodynamic polarization (corrosion current densities are given in parentheses), and (c) current–time transient results using glassy carbon, platinum wire, and SCE electrodes in 1 M $ZnSO_4$ electrolyte containing various MTU concentrations. (d) Surface morphology of Zn metal electrode soaked for 5 days in 1 M $ZnSO_4$ electrolyte containing various MTU concentrations. (e) Photographs of 1 M $ZnSO_4$ + 0.5 M MTU electrolyte contact angles on the Zn metal electrode.

electrolyte containing the MTU additive. Finally, the wetting properties were investigated using contact angle analysis. After dropping on the electrolyte with or without 0.5 M MTU (Fig. 2e), the contact angles on Zn metal were 29° and 36°, respectively. The easy change in the contact angle over time indicated that MTU imparted a more zincophilic property to the electrolyte.

First, MTU was compared with thiourea (TU), and then the optimal MTU concentration was determined by chronopotentiometry at a current density of 1 mA cm^{-2} (fixed at 1 mA h cm^{-2}) using Zn symmetric cells (Fig. S9 and S10†). The 0.05 M MTU concentration exhibited a stable charge–discharge behavior during the first few cycles, followed by a short circuit or overvoltage. However, this configuration was selected as the optimal concentration for all the subsequent studies since the electrochemical stability significantly increased with higher MTU concentrations, showing the lowest overvoltage and long-term stable cycling performance at 0.5 M. The cyclability of the Zn electrode with the MTU additive (Fig. 3a) was significantly extended, with stable cycling for over 1000 h, whereas the cell with bare $ZnSO_4$ showed voltage fluctuation and short circuits after 200 h due to severe side reactions. The Zn electrode with the MTU additive maintained a low voltage hysteresis of 58 and 77 mV at current densities of 3 and 5 mA cm^{-2}, respectively (Fig. 3b). This resulted in a uniform Zn plating/stripping behavior (Fig. S11†). Fig. 3c shows the Zn plating/stripping curves at current densities of 1–10 mA cm^{-2}. The overpotential increased only slightly without an internal short circuit when the current density increased, offering excellent rate performance in the electrolyte with MTU. The electrochemical performance was further evaluated by electrochemical impedance spectroscopy (EIS) measurements of the symmetric cells collected after the 50th cycle at a constant capacity of 1 mA h cm^{-2}. The Nyquist plot suggested that one semicircle was present, but there were two other smaller semicircles in the high- and low-frequency regions corresponding to surface resistance (R_{SEI}) and charge-transfer resistance (R_{ct}), respectively (Fig. 3d). The R_{SEI} and R_{ct} values for the symmetric cell without MTU were 10.7 and 35.9 Ω, respectively. This phenomenon was ascribed to the continuous decomposition reactions resulting from the contact between the Zn metal surface and the electrolyte. In contrast, the cell with MTU showed R_{SEI} and R_{ct} values of 3.2 and 5.8 Ω, respectively. This suggested that the MTU additive induced a stable formation of the interfacial layer and enhanced the electron-transport effect on the Zn plating/stripping layer.

X-Ray diffraction (XRD) and X-ray photoelectron spectroscopy (XPS) analyses were performed on the Zn metal electrodes after 10 and 50 cycles at a current density of 1 mA cm^{-2} to understand the uniformly dense interfacial layer of Zn metal by MTU. The diffraction peaks showed the phases assigned to Zn ($P6_3/mc$, ICDD no. 87-0713), ZnO ($P6_3mc$, ICDD no. 80-0075), and $Zn(OH)_2$ ($P2_12_12_1$, ICDD no. 76-1778), regardless of the use of MTU in the cell (Fig. S12 and S13†). The phases associated with the Zn passivation layer or dendrites exhibited no other obvious differences, except for the magnitude of the ZnO and $Zn(OH)_2$ reflection intensities. Therefore, *ex situ* XPS was used

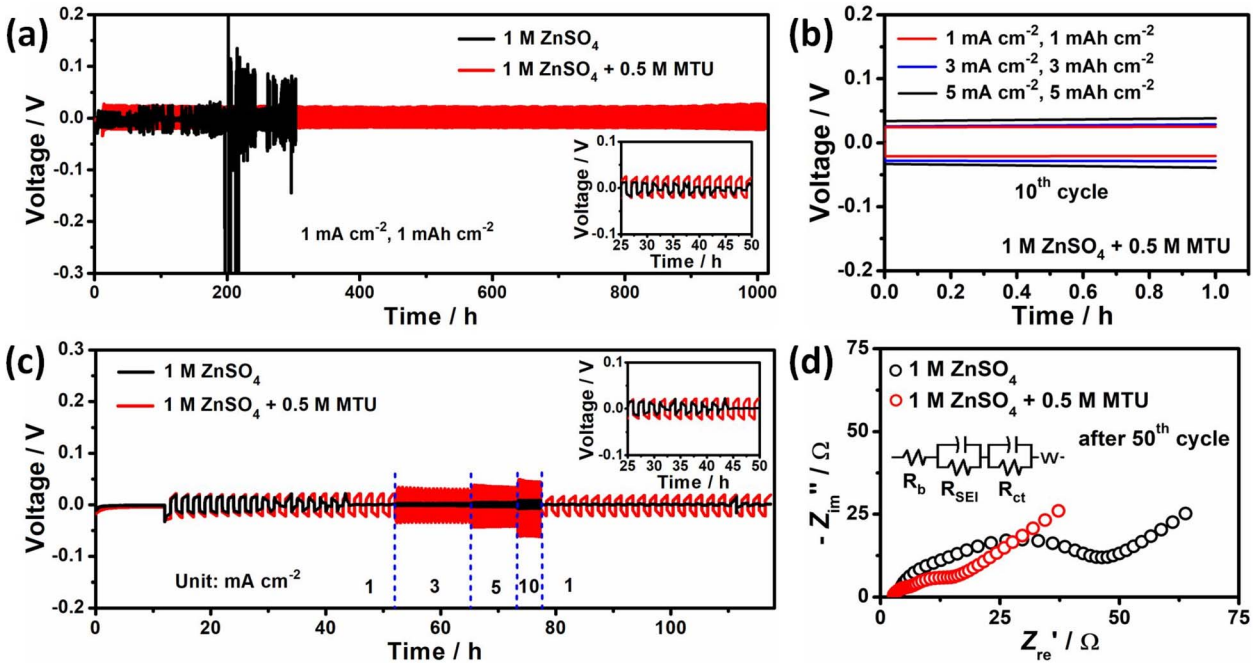

Fig. 3 (a) Chronopotentiometry results for Zn symmetric cells in 1 M $ZnSO_4$ electrolyte and 1 M $ZnSO_4$ + 0.5 M MTU electrolyte at 1 mA cm^{-2} with a cell capacity of 1 mA h cm^{-2}. (b) Detailed voltage profiles for Zn symmetric cells in 1 M $ZnSO_4$ + 0.5 M MTU electrolyte at 1, 3, 5 mA cm^{-2} with a capacity of 1, 3, 5 mA h cm^{-2} after 10 cycles. (c) Rate performance of Zn symmetric cells in 1 M $ZnSO_4$ electrolyte and 1 M $ZnSO_4$ + 0.5 M MTU electrolyte at current densities of 1, 3, 5, and 10 mA cm^{-2} with a fixed capacity of 1 mA h cm^{-2}. (d) Electrochemical impedance spectra of Zn symmetric cells in 1 M $ZnSO_4$ electrolyte and 1 M $ZnSO_4$ + 0.5 M MTU electrolyte after 50 cycles.

to determine the detailed chemical composition of the Zn metal electrode surface after 10 cycles. The high-resolution Zn 2p, O 1s, S 2p, and N 1s spectra are presented in Fig. 4a. The Zn 2p spectrum of the Zn metal electrode using MTU showed symmetric Zn $2p_{3/2}$ and $2p_{1/2}$ doublets associated with Zn(0) without a shift of the binding energy, and Zn^{2+} poor shoulder peaks related to ZnO (or $Zn(OH)_2$) at high binding energies.[45,46] While the Zn^{2+} shoulder was larger and more distinct in the Zn metal electrode without MTU. This indicated that MTU helped inhibit the formation of ZnO (or $Zn(OH)_2$) connected to Zn dendrites.[47,48] Further, the asymmetric O 1s spectrum was resolved into the peaks of Zn–O, H–O, and S–O bonds at 533.5, 532.5, and 532.2 eV, respectively.[49] The deconvoluted spectra may have originated from the Zn dendrites, adsorbed water, residual electrolyte salt, and MTU on the Zn metal surface. The Zn metal electrode using MTU showed decreases in the Zn–O and H–O bonds, probably due to the formation of relatively small dendrites and an increase in the S–O bond associated with MTU adsorption on the Zn metal surface. This was confirmed in the S 2p and N 1s spectra.[50,51] The amount of sulfur-related substances on the Zn metal surface (besides the $ZnSO_4$ salt in the electrolyte) was relatively high due to the adsorption of MTU. This was verified by the N–C and N–H bonds at 399.4 and 402.5 eV, respectively, in the N 1s spectra.[51] To further investigate the interaction between Zn ions and MTU, FTIR spectroscopy of the electrolyte was attempted after 50 cycles (Fig. S14†). The peaks at 1092, 1634, and 3242 cm^{-1} were associated with the absorption of SO_4^{2-}, bending vibration of adsorbed water, and –NH stretching vibration, respectively.[52–55] The absence of shifts in these peak positions after cycling indicates that the MTU is stable in the electrolyte without any reaction or decomposition by charging and discharging. Scanning electron microscopy (SEM) analysis after cycling and *in situ* optical visualization provided direct evidence for the effect of MTU additive on Zn metal in the electrolyte (in a lab-made cell, Fig. S15†). Non-uniform Zn dendrites in the shape of thin hexagonal platelets were formed on the Zn metal electrode without MTU in the surface SEM image of the Zn metal electrode after 150 cycles for the symmetric cell at 1 mA cm^{-2} (Fig. 4b). Even cell swelling occurred owing to the increase in pressure caused by the evolution of hydrogen gas and damage to the generated battery. In contrast, the Zn metal electrode containing MTU exhibited a change in the surface interfacial layer, which covered the surface with particles as small as 100 nm. In addition, even when the current density was increased to 3 mA cm^{-2} (Fig. S16†), the Zn metal surface was uniformly blanketed with small non-hexagonal particles with a size of ~200 nm. This change could be clearly confirmed in the real-time cycling electrode cross-sectional optical photo (Fig. 4c). In the absence of MTU, bubbles were generated by hydrogen evolution, and the electrode interface was changed to a rough and thick passivation layer owing to excessive dendrite formation. Meanwhile, the Zn metal electrode using MTU showed a uniformly dense passivation layer between the electrolyte and the Zn metal electrode (Fig. S17†). Based on the research findings, the role of the zinc/electrolyte interface reaction in the use of MTU additive is illustrated in Fig. 4d. In the 1 M $ZnSO_4$ electrolyte, many active H_2O molecules are

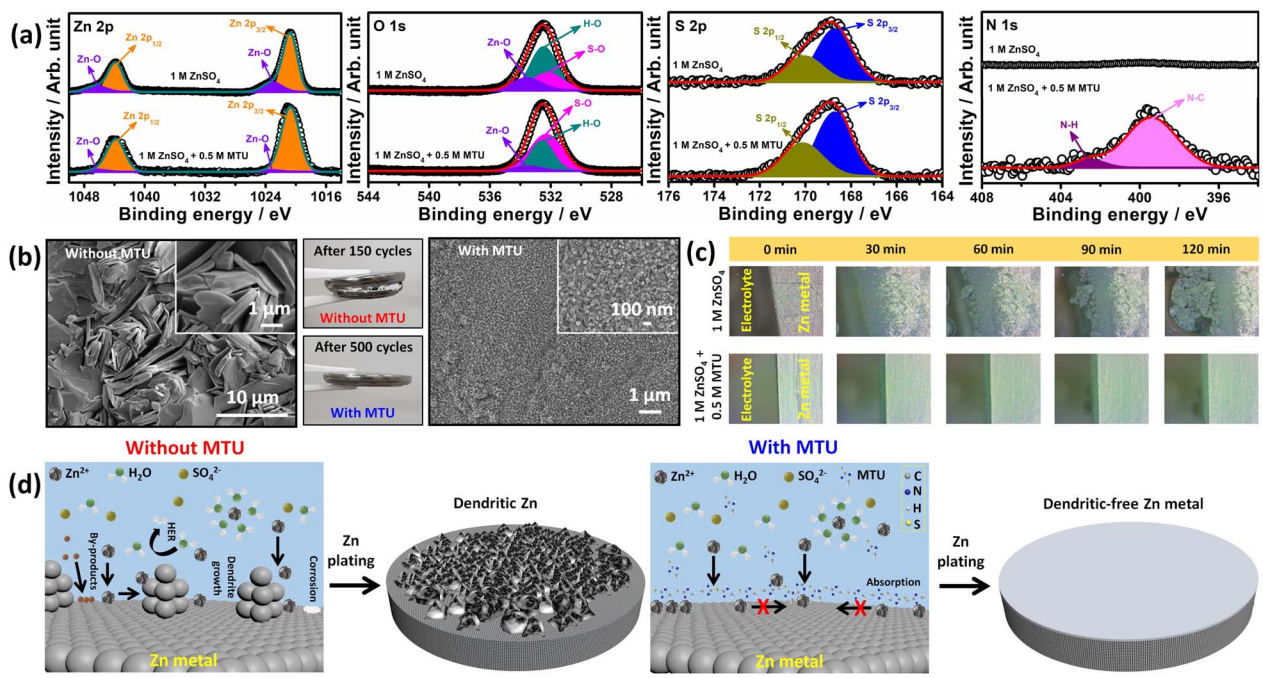

Fig. 4 (a) Zn 2p, O 1s, S 2p, and N 1s X-ray photoelectron spectra of Zn metal in 1 M $ZnSO_4$ electrolyte and 1 M $ZnSO_4$ + 0.5 M MTU electrolyte symmetric cells after 10 cycles. (b) SEM images of the Zn metal electrode surface behavior with and without MTU in 1 M $ZnSO_4$ electrolyte after 150 cycles. (c) Visualization of Zn-ion deposition on the Zn metal electrode with and without MTU by optical microscopy. (d) Schematic illustration of the Zn plating in 1 M $ZnSO_4$ with and without MTU electrolytes.

generated at the interface between the Zn metal and electrolyte, causing corrosion of the Zn electrode and growth of insulating by-products, finally inhibiting the reversible Zn plating/stripping. Conversely, introducing MTU with strong adsorption energy prevents the easy access of H_2O molecules to the Zn surface and suppresses the unwanted side reactions generated at the interface. Additionally, adsorbed Zn^{2+} ions during nucleation can limit the lateral diffusion behavior along the surface.

The effect of MTU adsorption at the electrode interface was evaluated by monitoring the open-circuit voltage decay that occurred by discharging a fully charged Zn|electrolyte with or without MTU|V_2O_5–C full-cells after 48 h of rest. A current density of 100 mA g^{-1} was used in the potential range of 1.5–0.8 V *vs.* Zn^{2+}/Zn. The XRD pattern of the V_2O_5–C cathode used for the evaluation is shown in Fig. S18† and the corresponding SEM images are shown in Fig. S19.† The cell using MTU eliminated the direct contact between the active Zn metal and the electrolyte and suppressed the interfacial side reactions (H_2 evolution and dendrites) during storage, thereby maintaining 94.9% of its original capacity (Fig. 5a). Meanwhile, it exceeded 72.9% in the Zn metal where MTU was not adsorbed. This phenomenon was presumed to be due to the formation of a stable interfacial layer where the Zn surface was functionalized by stable and favorable Zn^{2+} transport, which promoted reversible Zn stripping/plating. In the full-cell evaluation to confirm the practical use of the MTU additive, the first discharge and charge capacities at 100 mA g^{-1} of the Zn|electrolyte|V_2O_5–C full-cell to which MTU was applied were 220 and 210 mA h g^{-1}, respectively, and showed similar values even in the absence of MTU (Fig. 5b). The cycle performance stability of the cell with MTU delivered a consistent capacity over 420 cycles with a coulombic efficiency of ~98.6%. In contrast, the capacity of the cell without MTU sharply decreased to 83.9 mA h g^{-1} (capacity retention <48%) after 300 cycles, which mainly blocked Zn^{2+} interfacial transport by the formation of an insulating passivation layer, resulting in a large polarization. Moreover, the cell with MTU exhibited only a slight overpotential change during cycling at a high current density (1000 mA g^{-1}), and delivered considerable stability with a capacity retention of 92.8% and a coulombic efficiency of 99.7% for 300 cycles (Fig. S20†). This implied that the generation of a stabilized passivation layer could significantly increase the amount of charge passing through the cell. The feasibility of using MTU as an electrolyte additive for power-type Zn-ion batteries was further demonstrated by the rate capability of the cell. The cell containing MTU exhibited superior capacity characteristics with stable cycling compared to the cells without MTU at all current densities (Fig. 5c and d). There was only a slight increase in voltage in the cell with MTU when the current density was increased from 100 to 3000 mA g^{-1}. In contrast, there was a substantial increase in the voltage in the cell without MTU with the rising current density. In particular, the cell with MTU displayed a storage capacity of 106 mA h g^{-1} at 3000 mA g^{-1}, which was approximately five times that of the cell without additives. In addition, the cyclic voltammetry (CV) curves of the V_2O_5–C full-cell were measured at a scan rate of 0.1–0.5 mV s^{-1} and voltage range of 0.8–1.5 V *vs.* Zn^{2+}/Zn (Fig. S21†). Two well-separated redox peaks were exhibited at ~0.92/0.94 V and ~1.02/1.22 V. As the scanning speed increased, the distinct cathodic and anodic peaks did not coalesce and the full cell with MTU electrolyte exhibited smaller voltage gaps between the redox peaks. This indicated the better kinetics for Zn insertion and extraction. It was noteworthy that the stable passivation layer promoted a higher capacitive contribution to the Zn anode, resulting in fast electrochemical kinetics (Fig. S22†). The cells with MTU displayed higher Zn^{2+}-diffusion coefficient values than the cells without MTU over most of the charge process. This strongly suggested that the stable passivation layer created by the adsorbed MTU improved the kinetics of Zn-ion diffusion in the cell, leading to an excellent electrochemical performance.

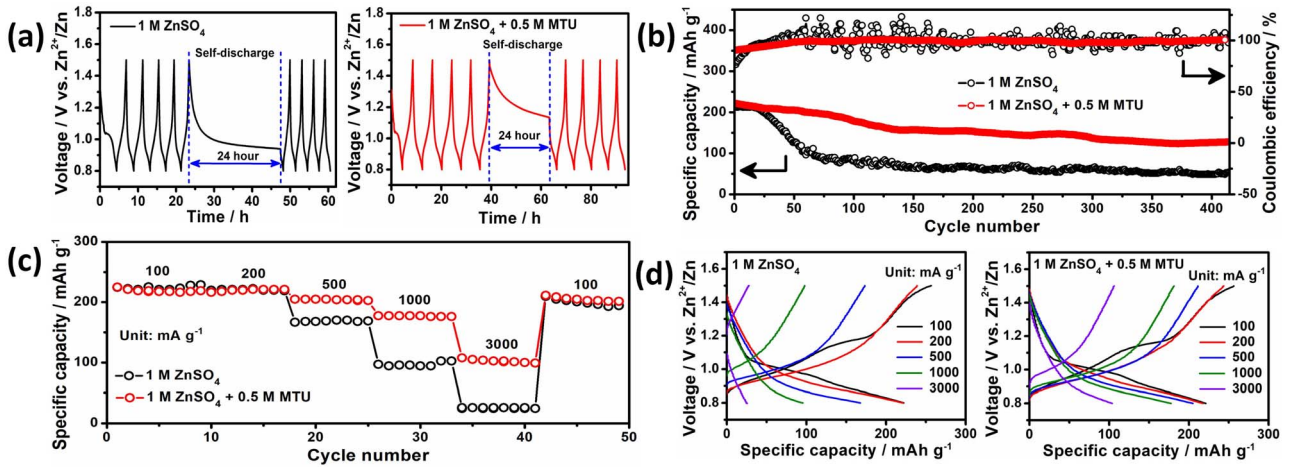

Fig. 5 (a) Storage performance in electrolytes with and without MTU by full discharge after 5 cycles at 100 mA g^{-1} and after 24 h rest at 100% charge. (b) Cycling performance including coulombic efficiency at 100 mA g^{-1}, (c) rate capacity and cycling retention, and (d) voltage profiles of full cell using V_2O_5–C composite cathode in 1 M $ZnSO_4$ electrolyte and 1 M $ZnSO_4$ + 0.5 M MTU electrolyte.

4 Conclusions

In summary, this is the first study to demonstrate an approach for achieving highly reversible Zn anodes by modulating the Zn metal interface *via* fertilizer-derived MTU adsorption. The adsorbed MTU molecules were induced to reduce the number of active sites on the electrode surface and prolong the induction time of Zn crystal formation. This resulted in the uniform deposition of Zn^{2+} ions on the Zn metal surface. In addition, the stable interfacial layer created by MTU adsorption greatly inhibited the side reactions and dendrite growth between the electrolyte and Zn metal. With this interface modulation, the symmetric cell in the electrolyte with MTU achieved stable cycling for 1000 h with a low polarization of 40 mV at 1 mA cm^{-2} and a capacity of 1 mA h cm^{-2}. Moreover, $Zn|V_2O_5$–C full-cells with the MTU electrolyte exhibited remarkable electrochemical reversibility, with a high-capacity retention of 98.6% for 420 cycles. This strategy is very effective in regulating metal nucleation and suppressing hydrogen evolution in aqueous electrolytes, and can help solve the dilemmas caused by the intrinsic properties of polyvalent metal anodes.

Author contributions

M. R. S. and S. Y. conceived the idea. M. R. S. carried out the materials synthesis, characterizations, and electrochemical tests. S. M. O. performed electrochemical tests. J. K. and K. Y. C. supervised the characterization section. M. R. S. wrote the original draft and J. K. revised the manuscript. K. Y. C. and S. Y. reviewed and refined the manuscript. All the authors discussed the results.

Conflicts of interest

There are no conflicts to declare.

Acknowledgements

This research was supported by the Basic Science Research Program through the NRF funded by the Ministry of Education (No. 2020R1I1A306182111) and Korea Institute for Advancement of Technology (KIAT) grant funded by the Korea Government (MOTIE) (P0017012, Human Resource Development Program for Industrial Innovation).

Notes and references

1 M. Winter, B. Barnett and K. Xu, Before Li ion batteries, *Chem. Rev.*, 2018, **118**, 11433–11456.
2 Y. Ding, Z. P. Cano, A. Yu, J. Lu and Z. Chen, Automotive Li-ion batteries: Current status and future perspectives, *Electrochem. Energy Rev.*, 2019, **2**, 1–28.
3 J. W. Choi and D. Aurbach, Promise and reality of post-lithium-ion batteries with high energy densities, *Nat. Rev. Mater.*, 2016, **1**, 16013.
4 J. Ming, J. Guo, C. Xia, W. Wang and H. N. Alshareef, Zinc-ion batteries: Materials, mechanisms, and applications, *Mater. Sci. Eng., R*, 2019, **135**, 58–84.
5 M. Song, H. Tan, D. Chao and H. J. Fan, Recent advances in Zn-ion batteries, *Adv. Funct. Mater.*, 2018, **28**, 1802564.
6 Z. Yi, G. Chen, F. Hou, L. Wang and J. Liang, Strategies for the stabilization of Zn metal anodes for Zn-ion batteries, *Adv. Energy Mater.*, 2021, **11**, 2003065.
7 L. E. Blanc, D. Kundu and L. F. Nazar, Scientific challenges for the implementation of Zn-ion batteries, *Joule*, 2020, **4**, 771–799.
8 W. Du, E. H. Ang, Y. Yang, Y. Zhang, M. Ye and C. C. Li, Challenges in the material and structural design of zinc anode towards high-performance aqueous zinc-ion batteries, *Energy Environ. Sci.*, 2020, **13**, 3330–3360.
9 J. Wang, Y. Yang, Y. Zhang, Y. Li, R. Sun, Z. Wang and H. Wang, Strategies towards the challenges of zinc metal anode in rechargeable aqueous zinc ion batteries, *Energy Storage Mater.*, 2021, **35**, 19–46.
10 Y. Song, P. Ruan, C. Mao, Y. Chang, L. Wang, L. Dai, P. Zhou, B. Lu, J. Zhou and Z. He, Metal-organic frameworks functionalized separators for robust aqueous zinc-ion batteries, *Nano-Micro Lett.*, 2022, **14**, 218.
11 Z. Xing, Y. Sun, X. Xie, Y. Tang, G. Xu, J. Han, B. Lu, S. Liang, G. Chen and J. Zhou, Zincophilic electrode interphase with appended proton reservoir ability stabilizes Zn metal anodes, *Angew. Chem., Int. Ed.*, 2023, **62**, e202215324.
12 Z. Huang, Z. Li, Y. Wang, J. Cong, X. Wu, X. Song, Y. Ma, H. Xiang and Y. Huang, Regulating Zn(002) deposition toward long cycle life for Zn metal batteries, *ACS Energy Lett.*, 2023, **8**, 372–380.
13 L. Kang, M. Cui, F. Jiang, Y. Gao, H. Luo, J. Liu, W. Liang and C. Zhi, Nanoporous $CaCO_3$ coatings enabled uniform Zn stripping/plating for long-life zinc rechargeable aqueous batteries, *Adv. Energy Mater.*, 2018, **8**, 1801090.
14 Q. Zhang, J. Luan, X. Huang, Q. Wang, D. Sun, Y. Tang, X. Ji and H. Wang, Revealing the role of crystal orientation of protective layers for stable zinc anode, *Nat. Commun.*, 2020, **11**, 3961.
15 Z. Cao, X. Zhu, D. Xu, P. Dong, M. O. L. Chee, X. Li, K. Zhu, M. Ye and J. Shen, Eliminating Zn dendrites by commercial cyanoacrylate adhesive for zinc ion battery, *Energy Storage Mater.*, 2021, **36**, 132–138.
16 L. T. Hieu, S. So, I. T. Kim and J. Hur, Zn anode with flexible β-PVDF coating for aqueous Zn-ion batteries with long cycle life, *Chem. Eng. J.*, 2021, **411**, 128584.
17 Y. Qin, P. Liu, Q. Zhang, Q. Wang, D. Sun, Y. Tang, Y. Ren and H. Wang, Advanced filter membrane separator for aqueous zinc-ion batteries, *Small*, 2020, **16**, 2003106.
18 Z. Yang, W. Li, Q. Zhang, C. Xie, H. Ji, Y. Tang, Y. Li and H. Wang, A piece of common cellulose paper but with outstanding functions for advanced aqueous zinc-ion batteries, *Mater. Today Energy*, 2020, **28**, 101076.
19 P. Cao, H. Zhou, X. Zhou, Q. Du, J. Tang and J. Yang, Stabilizing zinc anodes by a cotton towel separator for aqueous zinc-ion batteries, *ACS Sustainable Chem. Eng.*, 2022, **10**, 8350–8359.

20 B. Tang, L. Shan, S. Liang and J. Zhou, Issues and opportunities facing aqueous zinc-ion batteries, *Energy Environ. Sci.*, 2019, **12**, 3288–3304.
21 C. Liu, X. Xie, B. Lu, J. Zhou and S. Liang, Electrolyte strategies toward better zinc-ion batteries, *ACS Energy Lett.*, 2021, **6**, 1015–1033.
22 Y. Geng, L. Pan, Z. Peng, Z. Sun, H. Lin, C. Mao, L. Wang, L. Dai, H. Liu, K. Pan, X. Wu, Q. Zhang and Z. He, Electrolyte additive engineering for aqueous Zn ion batteries, *Energy Storage Mater.*, 2022, **51**, 733–755.
23 N. Wang, H. Wan, J. Duan, X. Wang, L. Tao, J. Zhang and H. Wang, A review of zinc-based battery from alkaline to acid, *Mater. Today Adv.*, 2021, **11**, 100149.
24 B. W. Olbasa, F. W. Fenta, S.-F. Chiu, M.-C. Tsai, C.-J. Huang, B. A. Jote, T. T. Beyene, Y.-F. Liao, C.-H. Wang, W.-N. Su, H. Dai and B. J. Hwang, High-rate and long-cycle stability with a dendrite-free zinc anode in an aqueous Zn-ion battery using concentrated electrolytes, *ACS Appl. Energy Mater.*, 2020, **3**, 4499–4508.
25 K. Zhao, F. Liu, G. Fan, J. Liu, M. Yu, Z. Yan, N. Zhang and F. Cheng, Stabilizing zinc electrodes with a vanillin additive in mild aqueous electrolytes, *ACS Appl. Mater. Interfaces*, 2021, **13**, 47650–47658.
26 H. Cao, X. Huang, Y. Liu, Q. Hu, Q. Zheng, Y. Huo, F. Xie, J. Zhao and D. Li, An efficient electrolyte additive of tetramethylammonium sulfate hydrate for Dendritic-Free zinc anode for aqueous Zinc-ion batteries, *J. Colloid Interface Sci.*, 2022, **627**, 367–374.
27 Y. Liu, Y. Li, X. Huang, H. Cao, Q. Zheng, Y. Huo, J. Zhao, D. Lin and B. Xu, Copper hexacyanoferrate solid-state electrolyte protection layer on Zn metal anode for high-performance aqueous zinc-ion batteries, *Small*, 2022, **18**, 2203061.
28 W. Xu, K. Zhao, W. Huo, Y. Wang, G. Yao, X. Gu, H. Cheng, L. Mai, C. Hu and X. Wang, Diethyl ether as self-healing electrolyte additive enabled long-life rechargeable aqueous zinc ion batteries, *Nano Energy*, 2019, **62**, 275–281.
29 H. Lu, X. Zhang, M. Luo, K. Cao, Y. Lu, B. B. Xu, H. Pan, K. Tao and Y. Jiang, Amino acid-induced interface charge engineering enables highly reversible Zn anode, *Adv. Funct. Mater.*, 2021, **31**, 2103514.
30 A. Bayaguud, X. Luo, Y. Fu and C. Zhu, Cationic surfactant-type electrolyte additive enables three-dimensional dendrite-free zinc anode for stable zinc-ion batteries, *ACS Energy Lett.*, 2020, **5**, 3012–3020.
31 K. O. Nayana and T. V. Venkatesh, Synergistic effects of additives on morphology, texture and discharge mechanism of zinc during electrodeposition, *J. Electroanal. Chem.*, 2011, **663**, 98–107.
32 K. E. K. Sun, T. K. A. Hoang, T. N. L. Doan, Y. Yu, X. Zhu, Y. Tian and P. Chen, Suppression of dendrite formation and corrosion on zinc anode of secondary aqueous batteries, *ACS Appl. Mater. Interfaces*, 2017, **9**, 9681–9687.
33 L. Cao, D. Li, E. Hu, J. Xu, T. Deng, L. Ma, Y. Wang, X.-Q. Yang and C. Wang, Solvation structure design for aqueous Zn metal batteries, *J. Am. Chem. Soc.*, 2020, **142**, 21404–21409.
34 F. Wang, O. Borodin, T. Gao, X. Fan, W. Sun, F. Han, A. Faraone, J. A. Dura, K. Xu and C. Wang, Highly reversible zinc metal anode for aqueous batteries, *Nat. Mater.*, 2018, **17**, 543–549.
35 C. Zhang, J. Holoubek, X. Wu, A. Daniyar, L. Zhu, C. Chen, D. P. Leonard, I. A. Rodríguez-Pérez, J.-X. Jiang, C. Fang and X. Ji, A $ZnCl_2$ water-in-salt electrolyte for a reversible Zn metal anode, *Chem. Commun.*, 2018, **54**, 14097–14099.
36 L. Wang, Y. Zhang, H. Hu, H.-Y. Shi, Y. Song, D. Guo, X.-X. Liu and X. Sun, A $Zn(ClO_4)_2$ electrolyte enabling long-life zinc metal electrodes for rechargeable aqueous zinc batteries, *ACS Appl. Mater. Interfaces*, 2019, **11**, 42000–42005.
37 Q. Han, X. Chi, Y. Liu, L. Wang, Y. Du, Y. Rend and Y. Liu, An inorganic salt reinforced Zn^{2+}-conducting solid-state electrolyte for ultra-stable Zn metal batteries, *J. Mater. Chem. A*, 2019, **7**, 22287–22295.
38 M. Yan, N. Dong, X. Zhao, Y. Sun and H. Pan, Tailoring the stability and kinetics of Zn anodes through trace organic polymer additives in dilute aqueous electrolyte, *ACS Energy Lett.*, 2021, **6**, 3236–3243.
39 X. Yang, S. Liu, J. Tang, G. Chang, Y. Fu, W. Jin, X. Ji and J. Hu, Effective inhibition of zinc dendrites during electrodeposition using thiourea derivatives as additives, *J. Mater. Sci.*, 2019, **54**, 3536–3546.
40 J. Yang, Y. Zhang, Z. Li, X. Xu, X. Su, J. Lai, Y. Liu, K. Ding, L. Chen, Y.-P. Cai and Q. Zheng, Three birds with one stone: Tetramethylurea as electrolyte additive for highly reversible Zn-metal anode, *Adv. Funct. Mater.*, 2022, **32**, 2209642.
41 M. K. Awad, Semiempirical investigation of the inhibition efficiency of thiourea derivatives as corrosion inhibitors, *J. Electroanal. Chem.*, 2004, **567**, 219–225.
42 Q. Zhang, Z. Yang, H. Ji, X. Zeng, Y. Tang, D. Sun and H. Wang, Issues and rational design of aqueous electrolyte for Zn-ion batteries, *SusMat*, 2021, **1**, 432–447.
43 Y. Song, J. Hu, J. Tang, W. Gu, L. He and X. Ji, Real-time X-ray imaging reveals interfacial growth, suppression, and dissolution of zinc dendrites dependent on anions of ionic liquid additives for rechargeable battery applications, *ACS Appl. Mater. Interfaces*, 2016, **8**, 32031–32040.
44 G. A. Giffin, The role of concentration in electrolyte solutions for non-aqueous lithium-based batteries, *Nat. Commun.*, 2022, **13**, 5250.
45 H. He, H. Tong, X. Song, X. Song and J. Liu, Highly stable Zn metal anodes enabled by atomic layer deposited Al_2O_3 coating for aqueous zinc-ion batteries, *J. Mater. Chem. A*, 2020, **8**, 7836–7846.
46 H. He and J. Liu, Suppressing Zn dendrite growth by molecular layer deposition to enable long-life and deeply rechargeable aqueous Zn anodes, *J. Mater. Chem. A*, 2020, **8**, 22100–22110.
47 Z. Li, S. Ganapathy, Y. Xu, Z. Zhou, M. Sarilar and M. Wagemaker, Mechanistic insight into the electrochemical performance of Zn/VO_2 batteries with an aqueous $ZnSO_4$ electrolyte, *Adv. Energy Mater.*, 2019, **9**, 1900237.

48 F. Wan, L. Zhang, X. Dai, X. Wang, Z. Niu and J. Chen, Aqueous rechargeable zinc/sodium vanadate batteries with enhanced performance from simultaneous insertion of dual carriers, *Nat. Commun.*, 2018, **9**, 1656.

49 B. W. Olbasa, F. W. Fenta, S.-F. Chiu, M.-C. Tsai, C.-J. Huang, B. A. Jote, T. T. Beyene, Y.-F. Liao, C.-H. Wang, W.-N. Su, H. Dai and B. J. Hwang, High-rate and long-cycle stability with a dendrite-free zinc anode in an aqueous Zn-ion battery using concentrated electrolytes, *ACS Appl. Energy Mater.*, 2020, **3**, 4499–4508.

50 X. Guo, Z. Zhang, J. Li, N. Luo, G.-L. Chai, T. S. Miller, F. Lai, P. Shearing, D. J. L. Brett, D. Han, Z. Weng, G. He and I. P. Parkin, Alleviation of dendrite formation on zinc anodes *via* electrolyte additives, *ACS Energy Lett.*, 2021, **6**, 395–403.

51 K. Xie, K. Ren, C. Sun, S. Yang, M. Tong, S. Yang, Z. Liu and Q. Wang, Toward stable zinc-ion batteries: Use of a chelate electrolyte additive for uniform zinc deposition, *ACS Appl. Energy Mater.*, 2022, **5**, 4170–4178.

52 L. Wang, G. Liu, L. Zou and D. Xue, Phase evolution from rod-like ZnO to plate-like zinc hydroxysulfate during electrochemical deposition, *J. Alloys Compd.*, 2010, **493**, 471–475.

53 J. M. Baruah, S. Kalita and J. Narayan, Green chemistry synthesis of biocompatible ZnS quantum dots (QDs): their application as potential thin films and antibacterial agent, *Int. Nano Lett.*, 2019, **9**, 149–159.

54 S. Habib, E. Fayyad, M. Nawaz, A. Khan, R. A. Shakoor, R. Kahraman and A. Abdullah, Cerium dioxide nanoparticles as smart carriers for self-healing coatings, *Nanomaterials*, 2020, **10**, 791.

55 J. Hao, L. Yuan, C. Ye, D. Chao, K. Davey, Z. Guo and S.-Z. Qiao, Boosting zinc electrode reversibility in aqueous electrolytes by using low-cost antisolvents, *Angew. Chem., Int. Ed.*, 2021, **60**, 7366–7375.

